JOURNAL OF CHEMICAL INFORMATION AND MODELING

Article

pubs.acs.org/jcim

Synthesis, Bioassay, and Molecular Field Topology Analysis of Diverse Vasodilatory Heterocycles

Polina V. Oliferenko,[¶] Alexander A. Oliferenko,[¶] Adel S. Girgis,[¶,‡] Dalia O. Saleh,[§] Aladdin M. Srour,[∥] Riham F. George,[⊥] Girinath G. Pillai,[¶,#] Chandramukhi S. Panda,[¶] C. Dennis Hall,*[,¶] and Alan R. Katritzky[¶,▽,○]

[¶]Department of Chemistry, University of Florida, Gainesville, Florida 32611-7200, United States

[‡]Pesticide Chemistry Department, [§]Pharmacology Department, and [∥]Therapeutical Chemistry Department, National Research Centre, Dokki, Cairo 12622, Egypt

[⊥]Pharmaceutical Chemistry Department, Faculty of Pharmacy, Cairo University, Cairo, Egypt

[#]Department of Chemistry, University of Tartu, Ravila 14a, Tartu 50411, Estonia

[▽]Department of Chemistry, King Abdulaziz University, Jeddah 21589, Saudi Arabia

Supporting Information

ABSTRACT: A diverse training set composed of 76 in-house synthesized and 61 collected from the literature was subjected to molecular field topology analysis. This resulted in a high-quality quantitative structure−activity relationships model (R^2 = 0.932, Q^2 = 0.809) which was used for the topological functional core identification and prediction of vasodilatory activity of 19 novel pyridinecarbonitriles, which turned out to be active in experimental bioassay.

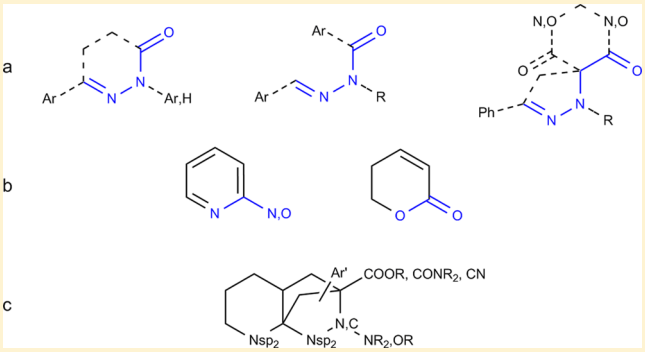

INTRODUCTION

Hypertension is a major risk factor for coronary heart and vascular diseases, stroke, and renal insufficiency which affects more than 26% of adults,[1,2] including some 65 million individuals in the United States.[3] Since the 1950s, when the first clinically useful antihypertensive drugs appeared, the strategy of such drug therapy has remained mainly unchanged, i.e., based on prevention of vasoconstriction or increased sodium excretion.[4] The development of new, more effective and selective antihypertensive drugs is of crucial importance for the treatment of hypertension as well as control of its prevalence.

Vasodilators are a large group of antihypertensive drugs which cause smooth muscle relaxation in blood vessels leading to a drop of arterial pressure. Vasodilating drugs are classified according to their primary mechanism of action such as α-adrenoceptor antagonists (quinazoline derivatives), calcium channel blockers (1,4-dihydropyridine-3,5-dicarboxylates), potassium channel openers (6-piperidin-1-ylpyrimidine-2,4-diamine-3-oxide), phosphodiesterase inhibitors (substituted 2-pyridinones, complex heterocyclic systems), nitrodilators, and others.[5] Nitrodilators such as the ubiquitous nitroglycerol were the first vasodilators widely used in clinical practice, but it was found long ago that nitroglycerol can only be administered for short periods of time because of rapidly developed tolerance. Experimental data on vasorelaxation activities are available for various chemical families of potent vasodilators.[6−12]

The chemical diversity of possible vasodilatory compounds is thus enormous. According to the literature, many heterocyclic families are or can be potent vasodilators, but any experimental, high-throughput screening is barely feasible because the chemical range spanned by potentially vasodilatory heterocycles is vast. A viable alternative to explore this huge chemically diverse space would be in silico analysis including quantitative structure−activity relationships (QSAR) and virtual screening. Notable accounts of computational vasodilatation activity modeling include: (i) linear discriminant analysis of resveratrol-coumarin hybrids;[13] (ii) pharmacophore mapping of pyridazinone derivatives;[14] (iii) 2D-QSAR modeling of flavonoids;[15] and (iv) 3D-pharmacophore and homology modeling studies of α_1-AR antagonists.[6d,e] The limited number of previous computational studies is, at least in part, due to the scarcity of available experimental data: only a few sources provide data numerous enough (at least 5−6 experimental data points per descriptor) for QSAR analysis. In the present work we advantageously use molecular field topology analysis (MFTA)[16] to explore the chemical space of existing and possible vasodilators and also to

Received: December 6, 2013
Published: February 16, 2014

Table 1. Experimentally measured and MFTA predicted IC_{50} (mM) values for 138 training set compounds

ID	Structure	IC_{50} exp.	IC_{50} pred.	ID	Structure	IC_{50} exp.	IC_{50} pred.	ID	Structure	IC_{50} exp.	IC_{50} pred.
1	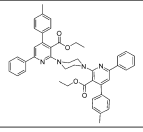	0.229	0.240	2	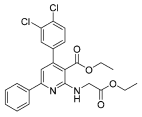	0.160	0.155	3	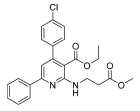	0.511	0.549
4	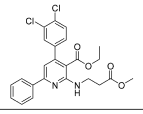	0.420	0.428	5	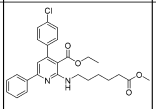	0.320	0.205	6	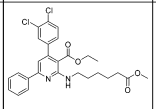	0.140	0.160
7	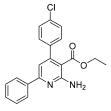	0.729	0.492	8	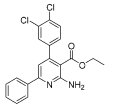	0.190	0.383	9	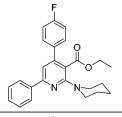	0.346	0.133
10	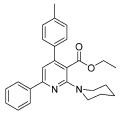	0.175	0.135	11	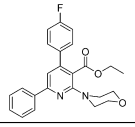	0.146	0.266	12	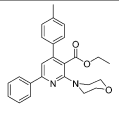	0.340	0.269
13	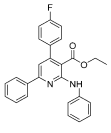	0.367	0.304	14	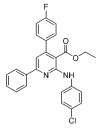	0.714	0.372	15	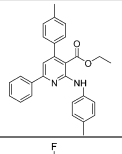	0.266	0.376
16	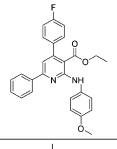	0.254	0.190	17	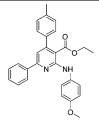	0.233	0.192	18	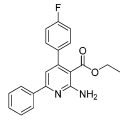	0.335	0.493
19	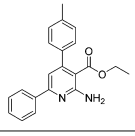	0.327	0.498	20	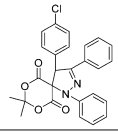	0.590	0.796	21	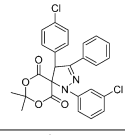	0.448	0.465
22	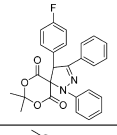	1.469	0.797	23	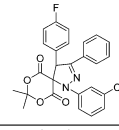	0.643	0.466	24	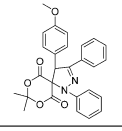	0.500	0.693
25	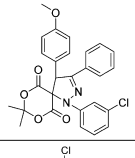	0.325	0.405	26	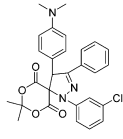	0.430	0.461	27	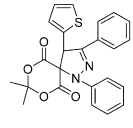	0.585	0.726
28	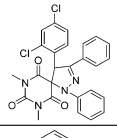	0.321	0.424	29	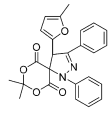	0.719	0.896	30	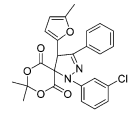	0.729	0.524
31	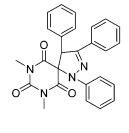	0.360	0.476	32	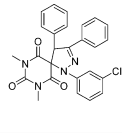	0.128	0.278	33	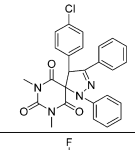	0.650	0.545
34	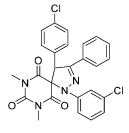	0.593	0.319	35	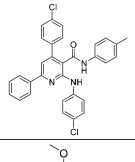	0.745	0.495	36	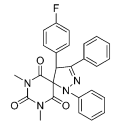	0.525	0.546
37	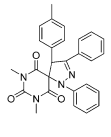	0.530	0.551	38	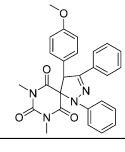	0.789	0.475	39	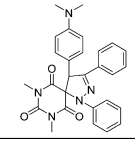	0.579	0.540

dx.doi.org/10.1021/ci400723m | J. Chem. Inf. Model. 2014, 54, 1103−1116

Table 1. continued

ID	Structure	IC_{50} exp.	IC_{50} pred.	ID	Structure	IC_{50} exp.	IC_{50} pred.	ID	Structure	IC_{50} exp.	IC_{50} pred.
40	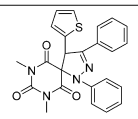	0.405	0.497	41	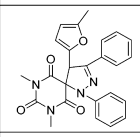	0.400	0.613	42	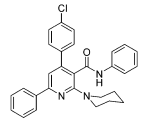	1.211	0.427
43	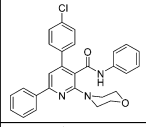	1.321	0.853	44	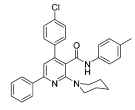	0.670	0.457	45	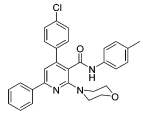	0.879	0.913
46	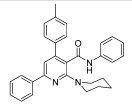	0.920	0.432	47	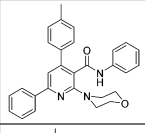	0.650	0.863	48	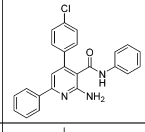	0.380	1.578
49	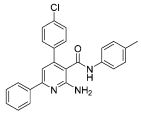	0.540	1.689	50	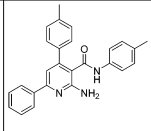	0.661	1.596	51	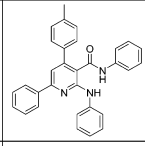	0.889	0.973
52	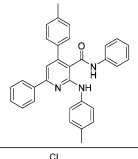	0.480	0.555	53	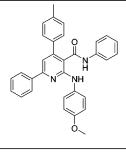	1.230	1.364	54	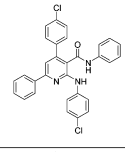	0.940	1.192
55	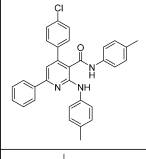	0.630	1.016	56	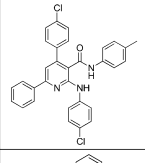	1.040	1.276	57	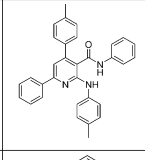	0.839	0.960
58	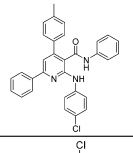	1.079	1.206	59	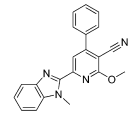	0.300	0.205	60	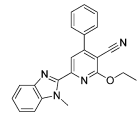	0.364	0.238
61	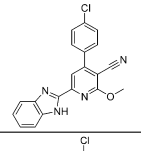	0.286	0.243	62	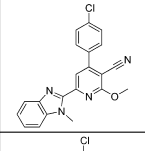	0.145	0.234	63	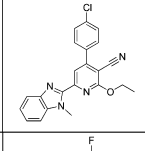	0.293	0.273
64	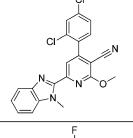	0.214	0.213	65	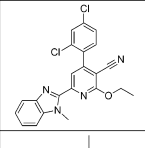	0.305	0.248	66	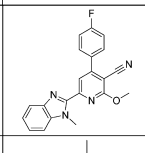	0.343	0.235
67	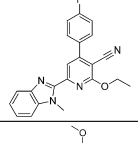	0.362	0.273	68	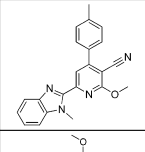	0.295	0.237	69	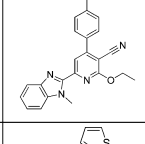	0.400	0.276
70	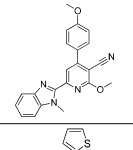	0.210	0.204	71	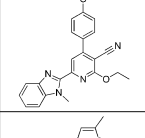	0.436	0.238	72	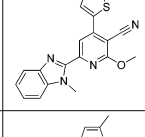	0.312	0.214
73	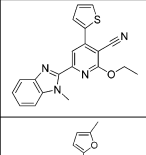	0.249	0.249	74	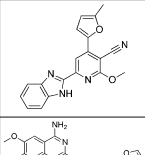	0.202	0.274	75	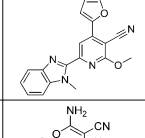	0.283	0.264
76	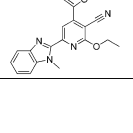	0.336	0.307	77	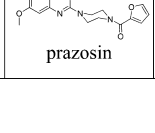 prazosin	0.488	0.343	78	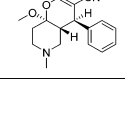	0.719	0.499

dx.doi.org/10.1021/ci400723m | J. Chem. Inf. Model. 2014, 54, 1103−1116

Table 1. continued

ID	Structure	IC_{50} exp.	IC_{50} pred.	ID	Structure	IC_{50} exp.	IC_{50} pred.	ID	Structure	IC_{50} exp.	IC_{50} pred.
91	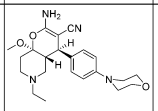	0.640	0.757	92	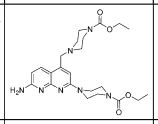	0.036	0.024	93	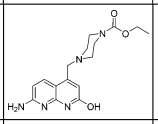	0.741	0.328
94	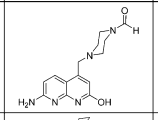	0.257	0.370	95	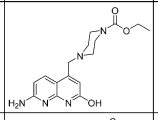	0.093	0.213	96	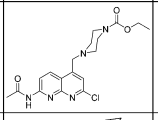	0.186	0.135
97	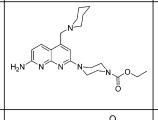	0.025	0.045	98	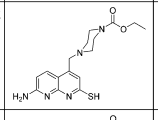	0.166	0.033	99	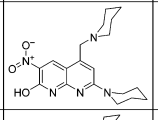	0.021	0.010
100	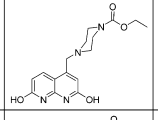	0.295	0.336	101	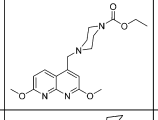	0.009	0.028	102	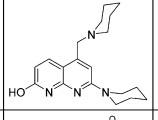	0.030	0.015
103	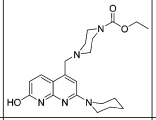	0.005	0.008	104	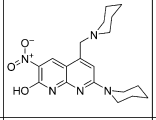	0.046	0.021	105	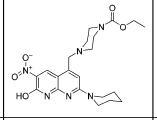	0.004	0.012
106	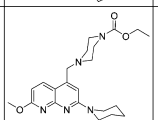	0.003	0.008	107	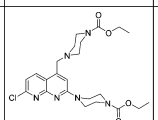	0.021	0.025	108	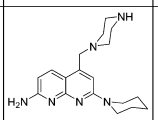	0.011	0.008
109	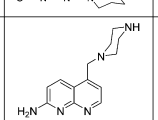	0.021	0.010	110	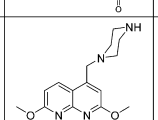	0.178	0.028	111	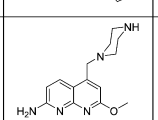	0.071	0.030
112	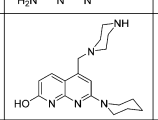	0.001	0.008	113	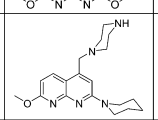	0.006	0.008	114	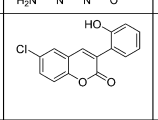	0.037	0.038
115	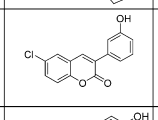	0.058	0.056	116	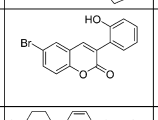	0.049	0.037	117	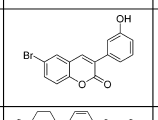	0.047	0.056
118	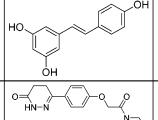	$31\cdot10^{-4}$	$14\cdot10^{-4}$	119	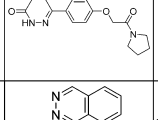	$13\cdot10^{-4}$	$5\cdot10^{-4}$	120	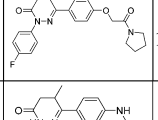	$1\cdot10^{-4}$	$3\cdot10^{-4}$
121	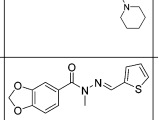	$13\cdot10^{-4}$	$7\cdot10^{-4}$	122	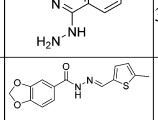	$3\cdot10^{-4}$	$37\cdot10^{-4}$	123	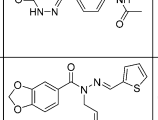	$1\cdot10^{-4}$	$3\cdot10^{-4}$
124	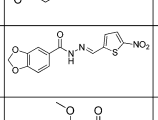	0.010	0.025	125	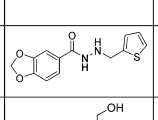	0.293	0.216	126	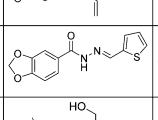	0.068	0.027
127	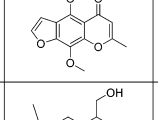	0.216	0.185	128	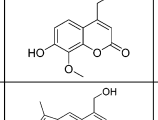	0.173	0.099	129	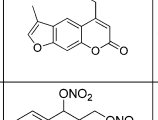	0.074	0.106
130	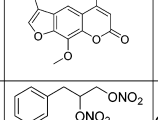	0.031	0.029	131		0.093	0.149	132		0.007	0.005
133		$42\cdot10^{-4}$	$45\cdot10^{-4}$	134		$52\cdot10^{-4}$	$43\cdot10^{-4}$	135		$25\cdot10^{-5}$	$3\cdot10^{-4}$
136		$6\cdot10^{-5}$	$1\cdot10^{-5}$	137		$18\cdot10^{-5}$	$13\cdot10^{-5}$	138		$5\cdot10^{-5}$	$3\cdot10^{-5}$

build predictive models accurate enough for further de novo design. MFTA is known to be a powerful QSAR method previously successfully applied to model various biological activities.[17−19]As a superposition technique, it is designed to find common fragments and thus to deal with an array of structurally diverse data sets. Previously published and new data recently obtained in our laboratories are collated to make up a combined diverse data set comprised of several heterocyclic

dx.doi.org/10.1021/ci400723m | J. Chem. Inf. Model. 2014, 54, 1103−1116

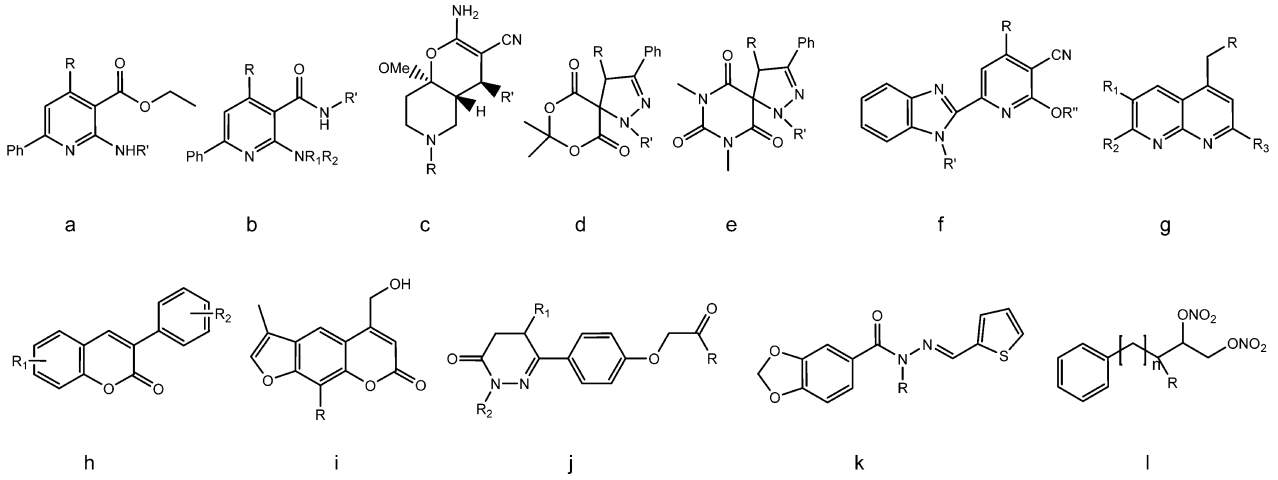

Figure 1. Compounds of the training data set: (a) 2-substituted-4,6-diaryl-3-pyridinecarboxylates, (b) 2-substituted-4,6-diaryl-3-pyridinecarbamides, (c) 4*H*-pyrano[3,2-*c*]pyridine-3-carbonitriles, (d) 7,9-dioxa-1,2-diaza-spiro[4,5]dec-2-ene-6,10-diones, (e) 1,2,7,9-tetraaza-spiro[4.5]dec-2-ene-6,8,10-triones, (f) 2-alkoxy-4-aryl-6-(1*H*-benzimidazol-2-yl)-3-pyridinecarbonitrile, (g) 1,8-naphthyridines, (h) phenylcoumarins, (i) furocoumarines, (j) pyridazinones, (k) *N*-acylhydrazones, (l) organic nitrates.

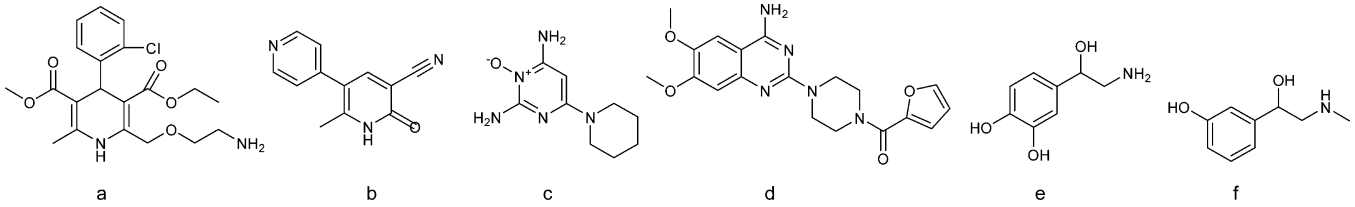

Figure 2. Some known vasodilator drugs structurally related to the training set compounds from Figure 1: (a) amlodipine, Ca^{2+} channel blocker; (b) milrinone, phosphodiesterase III inhibitor; (c) minoxidil, K^+ channel opener; (d) prazosin, α_1-adrenoreceptor antagonist. Vasoconstricor agents, class of α_1-adrenoreceptor agonists: (e) norepinephrine; (f) phenylephrine.

families possessing different mechanisms of action (pyridinecarboxamides **42**−**55** were previously reported by our group screened for their vasodilation properties and adopted as training set analogues, Table 1). The QSAR approach employed in this paper also suggests a pharmacophore hypothesis, in which a topological analogue of pharmacophore named a functional core is defined as a molecular subgraph occurring in all training set structures.

METHODS

Data set. Experimental data were collected on vasodilatation activity expressed as concentrations necessary for 50% reduction of maximal induced contracture, IC_{50}, as the measure most commonly used in pharmacological studies and thus more abundantly present in the literature. In all cases experimental data were obtained according to the same standard protocol: thoracic aortae of rats were precontracted by treatment with norepinephrine or phenylephrine, solutions of test compounds added, and relaxation response of aortae measured in a concentration-dependent manner. If original concentrations were given in units other than mM, they were recalculated before $-\log IC_{50}$ values were computed.

General structure patterns of training set compounds are shown in Figure 1, with numerical data summarized in Table 1. Compounds comprising the data set include: (i) 76 in-house synthesized nicotinate esters and amides,[6a−c] 2-amino-8*a*-methoxy-4*H*-pyrano[3,2-*c*]pyridine-3-carbonitriles,[6d] 7,9-dioxa-1,2-diaza-spiro[4,5]dec-2-ene-6,10-diones,[6e] 1,2,7,9-tetraaza-spiro[4.5]dec-2-ene-6,8,10-triones,[20] and 2-alkoxy-4-aryl-6-(1*H*-benzimidazol-2-yl)-3-pyridinecarbonitriles[21] and (ii) 61 data points collected from the literature, namely 1,8-naphthyridine,[7] furocoumarin,[11] phenylcoumarin,[8,22] 4,5-dihydro-3(2*H*)-pyridazinone, *N*-acylhydrazone,[10] and organic nitrate derivatives.[12]

The mechanisms of action of these compounds have not yet been fully identified, but the possibility exists that they have the same origin as those of some known structurally related vasorelaxing agents. For example, nicotinamide can inhibit directly vascular smooth muscle cell contraction by calmodulin, myosin light chain kinase, and adenylate cyclase activation[23] or induce vasodilation through binding with specific nicotinic acetylcholine receptors, which results in release of adrenergic neurotransmitters and nitric oxide.[24,25] A class of structurally very similar 1,4-dihydropyridine-3,5-dicarboxylate vasosilators (amlodipine, manidipine, felodipine, etc., see Figure 2) are calcium channel blockers stimulating emission of nitric oxide as well.[26] Antihypertensive activity of 1-oxa-4,9-diazaspiro[5.5]-undecan-3-ones structurally related to 7,9-dioxa-1,2-diaza-spiro-[4,5]dec-2-ene-6,10-diones and 1,2,7,9-tetraaza-spiro[4.5]dec-2-ene-6,8,10-triones is due predominantly to peripheral α_1-adrenergic blockade.[27]

As for the compounds collected from the literature (**78**−**138**), their modes of action can be rather diverse. Thus, there is evidence that various 1,8-naphthyridines can act as guanilate-cyclase inhibitors, potassium channel openers,[7] and α_1-adrenoceptor antagonists.[28] Vasorelaxing potency of pyridazinone and *N*-acylhydrazone derivatives is explained by their ability to inhibit phosphodiesterase types III[14] and V,[29] respectively. The effect of furocoumarins may be related to Ca^{2+} agonist activity and enhancement of prostaglandins release.

dx.doi.org/10.1021/ci400723m | *J. Chem. Inf. Model.* 2014, 54, 1103−1116

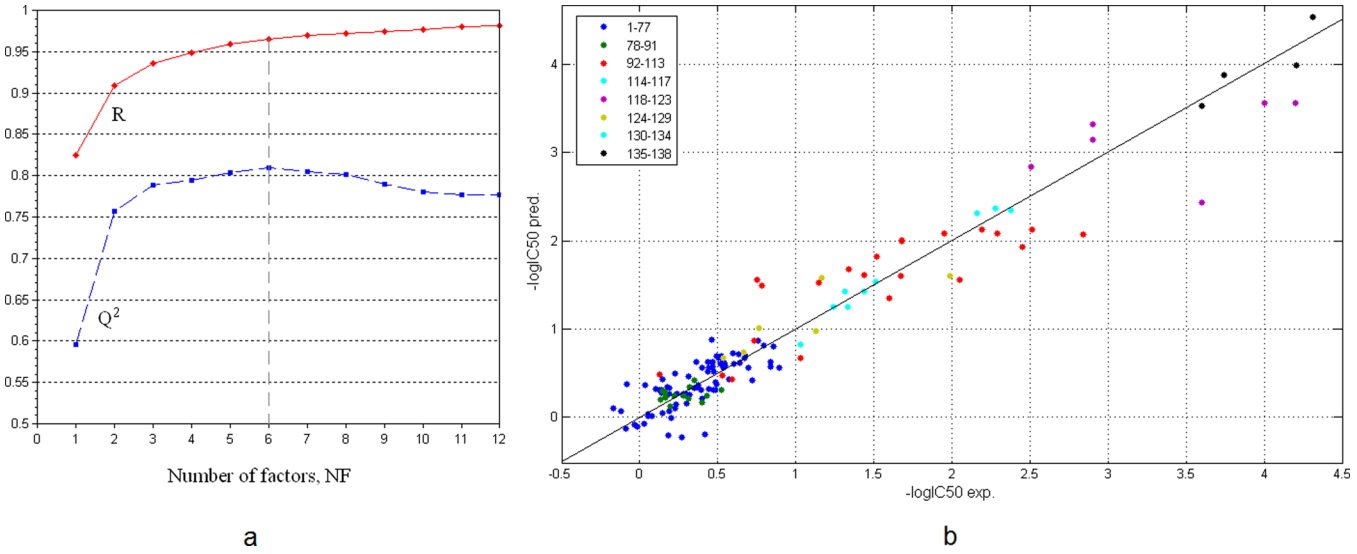

Figure 3. Characteristics of the MFTA model obtained for the overall set of 138 compounds: (a) factor dynamics plot for correlation coefficient *R* and cross-validation $Q_{10\%}^2$ and (b) "observed vs predicted" fitting plot (right). Seven chemotypes of vasodilators are marked in different colors.

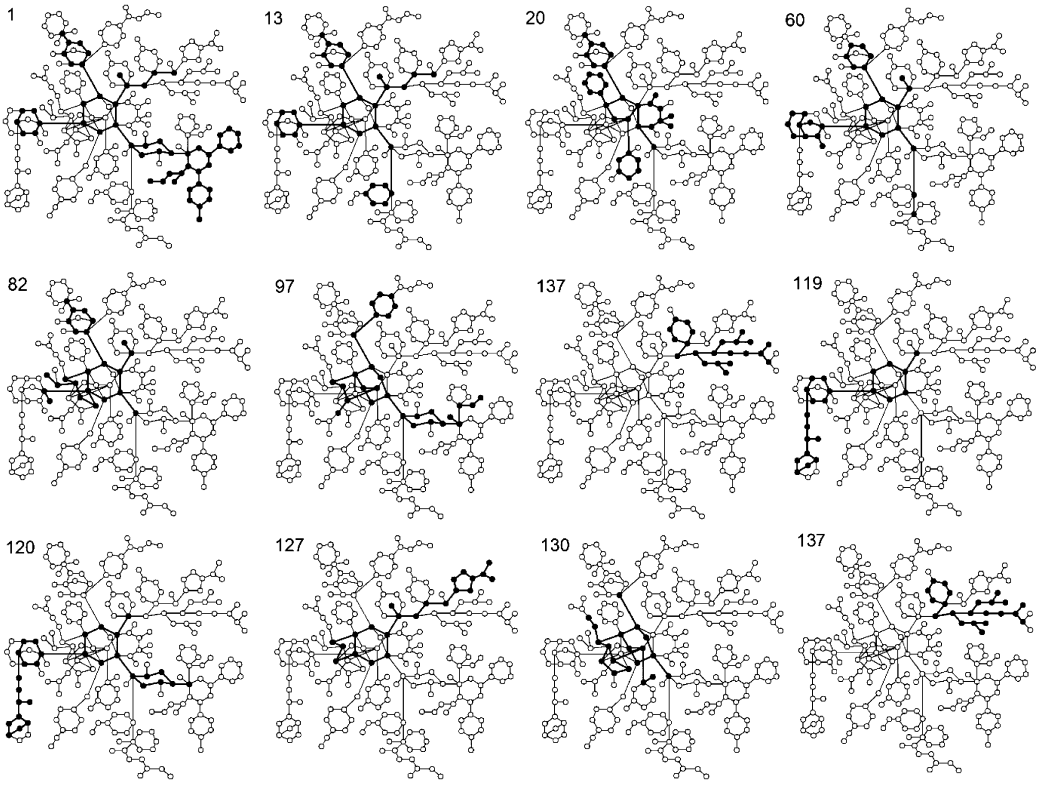

Figure 4. MSG built for the training data set of 138 structures with representative superimposed molecules. The numbers correspond to the numbers of the molecules in Table 1.

Finally, a group of nitrodilators, organic nitrates, is suggested to undergo an enzymatic processing to release NO, an important endothelial-derived smooth muscle relaxing agent with multiplex vascular functions.

Molecular Field Topology Analysis. MFTA is an analytical tool for the construction of quantitative structure−activity relationships of structurally related compounds. It considers structural similarity both locally (when specific subgraphs within the two molecular graphs are compared) and globally (when two molecular graphs are compared). MFTA represents molecular structures in the form of molecular graphs, which are subsequently superimposed onto the emerging molecular supergraph. The ultimate shape of the two-dimensional molecular supergraph (MSG) takes into account the commonality of distinct common scaffolds as well as of disjoint parts of the molecules. The MSG vertices and edges correspond to the atoms and bonds, respectively, and are assigned the values of local descriptors, which are then processed further by partial least-squares regression to obtain a structure−activity model. The descriptor pool utilized includes charge, electronegativity,

dx.doi.org/10.1021/ci400723m | J. Chem. Inf. Model. 2014, 54, 1103−1116

hydrogen bonding, van der Waals radius, lipophilicity, and electrotopological descriptors. The predictive quality of a model is characterized by the squared correlation coefficient, R^2, and the cross-validation parameter Q_n^2, where n is a user-defined parameter for the number of structures in a test set.

RESULTS AND DISCUSSION

MFTA Modeling. The MFTA structure−activity model, generated for 138 compounds of the training set, includes five molecular fields or descriptors: Gasteiger−Marsili atomic charges, van der Waals radii, local atomic lipophilicities, and hydrogen-bond acceptor and donor scales.

The factor dynamics and "observed vs predicted" fitting plots are shown in Figure 3. As can be seen in Figure 3a, both the correlation coefficient R and the squared cross-validation coefficient Q^2 grow almost in parallel until the number of components reaches six: above this, Q^2 starts to exhibit a decrease as the number of the factor increases. When six factors were taken into account, the squared correlation coefficient was $R^2 = 0.932$ and the predictive ability characterized by a 10%-out cross-validation, $Q_{10\%}^2$, was 0.809, with the mean unsigned error equal to 0.187.

The data points on the correlation plot shown in Figure 3b are marked in different colors to distinguish between the seven chemotypes. As can be seen, chemical classes fall roughly into two subgroups: a more compact arrangement of less active compounds and less numerous points with higher pIC_{50} values. One can clearly see that naphthiridines cover the range of more than 2.5 log units and that each of the seven chemotypes overlap with at least two others, except for organic nitrates, which overlap only with the pyridazinone series. Taken together, the data form a smooth and evenly distributed outline spanning over almost 5.0 logarithmic units.

The molecular supergraph, constructed by the superimposition of all the training set structures, is shown in Figure 4 along with examples of superimposed structures. As expected, the MSG is complex because of the high diversity of the constituent molecules. As can be seen, the molecular subgraphs of all chemical groups except organic nitrates have at least one fragment shared with two or more other subgraphs, which attests to the overall consistency of the MSG. Such an even character of subgraphs superimposition leads to an equivalently even manifestation of the features thereof. This opens up an opportunity to suggest new prospective vasodilators by the analysis of the MSG's different fragments along with the descriptor contributions (see Interpretation of MFTA Models section).

As MFTA was applied for a heterogeneous data set composed of different chemotypes with presumably diverse mechanisms of action, one can find it highly relevant to compare the prediction quality of the general MFTA model with that of the models built for each individual chemotype. Thus, a separate MFTA model was generated for a subset of 54 pyridine derivatives (#1−#19, #42−#76) including pyridinecarboxylates, pyridinecarbamides, and pyridinecarbonitriles. The statistical quality was the best with two factors: $R^2 = 0.675$, $Q_{10\%}^2 = 0.600$; mean unsigned error equal to 0.117. Another two-factor model was built for 22 naphthiridines: $R^2 = 0.778$, $Q_{10\%}^2 = 0.619$; mean unsigned error 0.259. So, the general MFTA model statistically outperforms the individual chemotype models, which supports validity of the choice to build a single general, heterogeneous MFTA model rather than several focused ones.

Interpretation of MFTA Models. A distinguishing feature of MFTA and similar 2D and 3D-QSAR methods is that they employ local characteristics versus whole-molecule descriptors used in multiple-regression-based QSAR/QSPR approaches. As a result, a target activity is interpreted in terms of vectors rather than constants, i.e., it can be regulated by increasing or decreasing particular atomic parameters by replacing one atom by another or changing nearest neighborhood.

The impacts of molecular fields or descriptors on the general model are reflected by two-colored images displayed in Figure 5.

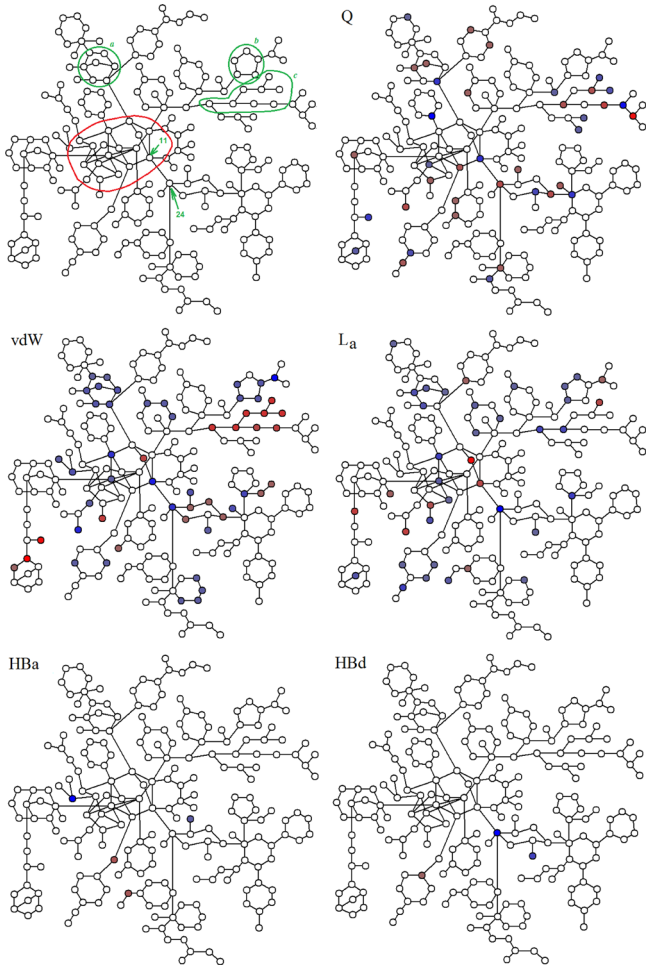

Figure 5. Relative impacts of the molecular fields on the title activity for the model built on 138 data points: atomic charge (Q), atomic van der Waals radius (vdW), hydrogen-bond acceptor (HB_a), hydrogen-bond donor (HB_b), and atomic lipophilicity (L_a). Red and blue colors indicate, respectively, increase or decrease of local descriptor values that enhance the target activity. Positions discussed in the text are marked in green in MSG. The red circle indicates the position of the functional core.

Red color indicates that an increase of a local descriptor value leads to an enhancement of activity, whereas blue color denotes that magnification of activity can be achieved by a decrease of the local descriptor value. As was mentioned earlier, merging of local influences which pertain at least three different structural fragments significantly complicates analysis of individual influences, but it is a beneficial factor for the development of novel, potentially active agents.

Visual analysis of the MSG images shown in Figure 5 reveals a mutual correlation between descriptor impacts at certain

dx.doi.org/10.1021/ci400723m | J. Chem. Inf. Model. 2014, 54, 1103−1116

positions. For example, concurrent rendering of position 11 in blue for electrostatic (Q) and steric (vdW) fields and in red for lipophilicity (L_a) field indicate that a more negative charge, a smaller volume and higher atomic lipophilicity are preferable at this location. Taking into account that position 11 is occupied by carbon and nitrogen atoms and comparing respective descriptor values in Table 2 suggest that an sp^3-hybridized heterocyclic

Table 2. Descriptor Values for the Atom Types Occupying Position 11 of the MSG

atom type	Q	vdW	L_a
$C_{sp^2(\text{benzyl ring})}$	0.0614; −0.0010; −0.015	1.7	−0.1378; −0.0548
$C_{sp^2(C=O)}$	0.1577	1.7	−0.1703
$N_{sp^3(\text{heterocycle ring})}$	−0.0923	1.55	0.1414
N_{sp^2}	−0.0623	1.55	0.1757

nitrogen atom is more favorable than an sp^2-hybridized carbon atom. High activities of pyridazinones (str. **119**−**123**) with the N_{sp^3} atom in position 11 (see structure **120** in Figure 4) serve as a good validation of this conclusion.

An opposite situation is observed for position 24, which demands a concurrent increase in atomic charge and a decrease in atomic volume and lipophilicity, while being populated by a variety of atomic types (see Table 3 for details). At the same time

Table 3. Descriptors for the Atom Types Occupying Position 24 of the MSG

atom type	Q	vdW	L_a	HB_d
NH_2	−0.139	1.55	0.141	0.6
$N_{sp^3(\text{cycle})}$	−0.132	1.55	0.141	−2.00
$O_{sp^3(-OCH3)}$	−0.198	1.52	0.341	−2.00
$O_{sp^2(C=O)}$	−0.109	1.5	−0.173	−2.00
OH	−0.204	1.52	0.521	2.10
Cl	−0.0873	1.75	0.697	−2.00
SH	−0.058	1.8	1.015	−2.00
CH_3	−0.025	1.7	−0.633	−2.00

the presence of hydrogen-bond donors such as hydroxyl and amino groups are not beneficial, as indicated by the strong blue hue of position 24 on the hydrogen-bond donor field. According to the data in Table 3, the CH_3 group has the optimum combination of all four descriptor values.

Other informative parts in the MSG descriptor images are the conglomerates of adjacent five- and six-membered rings marked with *a* and *b* for simplicity. Ring *a* is constructed by superimposition of aryl fragments of 3-pyridinecarboxylates, 3-pyridinecarbamides, and 3-pyridinecarbonitriles as well as thienyl and furanyl rings in spiro compounds. Predominance of the blue hue for steric and lipophilic fields attests that less bulky and less lipophilic systems are more beneficial compared to aromatic hydrocarbon cores. Similar features are observed in color rendering of the *b* ring occupied particularly by a thienyl fragment in *N*-acylhydrazones. Analysis reveals that aliphatic carbon atoms are preferred compared to the benzene and five-membered rings, because they are smaller and lipophilic. The overall analysis of steric and lipophilic characteristics of the fragment *c* suggests that an aliphatic C_5−C_6 linear moiety ending up with a bulky electronegative group could contribute better to the target activity. Such a moiety is present in organic nitrates which, as shown in Figure 4 (str. **137**), are superimposed onto this particular section of the MSG. Based on these conclusions, one can hypothesize an efficiency of a bulky substituent in pyridine-3-carboxylates and pyridine-3-carboxamides, which contain a strong negatively charged fragment such as nitro or nitrate group.

Identification of Topological Functional Core (Pharmacophore). All classes of compounds comprising the training set presumably have different modes of action, which do not have much in common at least from the topological point of view. Based on the MFTA models described above, one can deduce a functional core center from the MSG structures. Here we can speak about a topological analog of a pharmacophore, because MFTA superimposes structures in the topological or graph-theoretical way. The notion of topological pharmacophore can be formulated differently. The very first definition probably goes back to the early work of Franke et al.,[30] where a "topological pattern" or "topological pharmacophore" was regarded as "an ensemble of structural features that is characteristic of a group of compounds possessing a desired biological property". Another definition is based on pairwise topological distances proposed by Schneider[31] to account for isofunctionality of structurally distant compounds. Bonachera et al. applied fuzzy logic to define tricentric pharmacophore descriptors.[32] The field of topological pharmacophore and its application in drug design was comprehensively reviewed by Horvath in Chapter 2 of "Chemoinformatics Approaches to Virtual Screening".[33] We define a topological functional core as a subgraph (not necessarily smallest) of the MFTA molecular supergraph, which is common in all training set structures. This definition is related to the clique or a "maximal completely connected graph", but because of heuristic assumptions is not as rigorous as the definition of clique.

Analysis of vasodilators in Figure 2 and structures in the data set together with their superimpositions on the MSG exemplified in Figure 4 enables one to define the key structural elements common to all molecules. One of them is the structural motif shown in blue in Figure 6a. This motif is present in pyridazinones

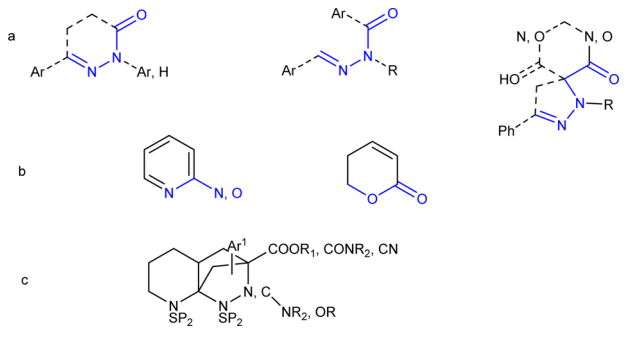

Figure 6. (a,b) Structural fragments common for molecules of the training data set. (c) Topological functional core proposed on the basis of MFTA molecular supergraph and descriptor field's analysis.

and *N*-acylhydrazones; a very similar motif can be found in diazaspiro and tetraazospiro compounds. The second commonly met and partially overlapping with the first motif is the combination shown in Figure 6b; it is incorporated in the molecular core of 3-pyridinecarboxamides, 3-pyridinecarboxylates, 3-pyridinecarbonitriles, 4*H*-pyrano[3,2-*c*]pyridine-3-carbonitriles, 1,8-naphthyridines, and furocoumarines. All these fragments concurrently superimposed on the MSG within the same topological area are marked on Figure 5 with a red circle.

dx.doi.org/10.1021/ci400723m | J. Chem. Inf. Model. 2014, 54, 1103−1116

We define this fragment as a common topological pattern or topological functional core.

The topological functional core shown in Figure 6c embraces the whole general data set of 138 compounds. It was derived from analysis of the above supergraph as well as the chemical structures themselves. This core consists basically of a fused bicyclic fragment enriched with heteroatoms. It also includes functional groups in the immediate vicinity of the bicyclic fragment, which imparts not only topological but also chemical similarity. On this graph R stands for alkyl substituents and Ar^1 is the aryl or other bulky substituent which contains an alkyl chain with a strong electronegative group at the end, such as nitro or carboxyl group. This functional core may or may not be the only possible one, but it demonstrates a good quality QSAR, as represented by $R^2 = 0.932$ and $Q^2 = 0.809$. The goal of deriving such a functional core is not prediction per se but rather a starting point for de novo design by combining a common topological pattern with favorable structural features inherited from various chemotypes.

Prediction of Vasodilatory Activity with the MFTA Model. MFTA model was applied to the prediction of vasodilatory activity of 19 newly synthesized thienyl-nicotinonitrile derivatives. Experimental and predicted values are given in Table 4. Three most active compounds, **147**, **153** and **154**, have vasodilatory activities with the IC_{50} values equal to 0.066, 0.084, and 0.045 mM, respectively. As can be seen, the predicted values match quite well the experimental data, with the exception of compounds **147** and **152** which have errors more than 0.290 mM. Four out of 19 predicted values deviated from the experimental ones at higher than 0.1 mM (compounds **148**, **149**, and **165** reveal error in their IC_{50} values 0.255, 0.137, and 0.181, respectively). The correlation itself between experimental and predicted values for all 19 compounds turned out to be low, but upon removal of two major outliers (compounds **147** and **152**), the correlation coefficient significantly improved to 0.620.

As all the synthesized compounds in the test set belong to the same chemotype, it was suggested highly relevant to predict their activities using the model built on a smaller training set of 54 pyridine derivatives (#1−#19, #42−#76), including pyridinecarboxylates, pyridinecarbamides, and pyridinecarbonitriles. The statistical quality of this model was the highest when two factors were taken into account: $R^2 = 0.675$, $Q^2 = 0.600$, and the mean unsigned error was equal to 0.117. Prediction of activities for 19 thienyl-nicotinonitrile derivatives using the model for 54 pyridine compounds turned out to be much inferior to the general model shown in Figure 3, even after outliers **147** and **152** were excluded.

As a result, the use of a large diverse data set gives a better predictive model for the test set compounds compared to using the focused, chemotype-specific training sets. This brings evidence that the proposed MFTA model can be reliably applied to the prediction of vasodilatory activity of novel chemical structures.

Table 4. Predicted Vasodilatory Activity IC_{50} (mM) for 17 Thienyl-Nicotinonitrile Derivatives

ID	Structure	$IC_{50exp.}$	$IC_{50pred.}$	error	ID	Structure	$IC_{50exp.}$	$IC_{50pred.}$	error
147	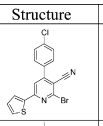	0.066	0.430	0.364	**148**	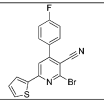	0.176	0.431	0.255
149	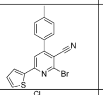	0.288	0.425	0.137	**150**	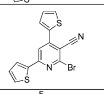	0.297	0.378	0.081
151	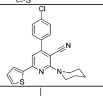	0.152	0.123	0.029	**152**	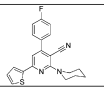	0.421	0.124	0.297
153		0.084	0.122	0.038	**154**		0.045	0.109	0.064
155	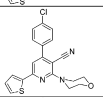	0.168	0.230	0.062	**156**	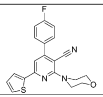	0.197	0.230	0.033
157	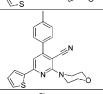	0.128	0.227	0.099	**158**	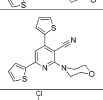	0.166	0.202	0.036
159	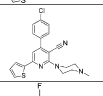	0.240	0.185	0.055	**160**	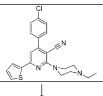	0.197	0.233	0.036
161	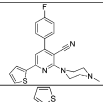	0.145	0.185	0.040	**162**	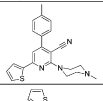	0.140	0.183	0.043
163	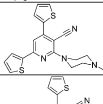	0.201	0.163	0.038	**164**	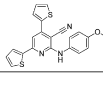	0.157	0.096	0.061
165	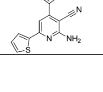	0.159	0.339	0.181					

SYNTHESIS

Compounds **31**−**41**[20] and **42**−**58**[6b] were prepared according to previously reported procedures, and their vasodilation activities were determined by standard techniques.[6a,c−e] The targeted 6-(2-thienyl)-3-pyridinecarbonitriles **147**−**165** were synthesized according to the synthetic procedures shown in Schemes 1 and 2.

Scheme 1. Synthetic Route Towards 2-Bromo-3-pyridinecarbonitriles

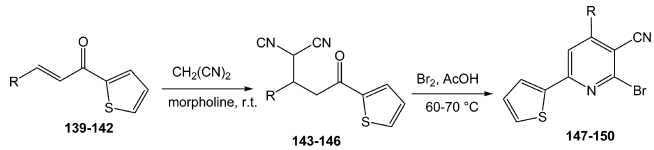

139, 143, 147; R = 4-ClC_6H_4

140, 144, 148; R = 4-FC_6H_4

141, 145, 149; R = 4-$H_3CC_6H_4$

142, 146, 150; R = 2-thienyl

A mixture of equimolar amounts of 1,3-diaryl-2-propen-1-ones **139**−**142** with malononitrile in ethanol in the presence of morpholine as a basic catalyst at room temperature afforded the corresponding (1,3-diaryl-3-oxo-propyl)propanedinitriles **143**−**146** in good yields (81−89%). The structure of **143**−**146** was established through spectroscopic (IR, ^{1}H NMR) and elemental analysis. The IR spectra of **143**, as a representative example of this family, revealed the presence of a ketonic carbonyl function at $\nu = 1653$ cm^{-1} plus a nitrile stretching vibration band at $\nu = 2260$ cm^{-1} confirming isolation of the open-chain Michael adduct product. ^{1}H NMR spectrum of **143** showed the propyl methylene H_2C-2 as a diastereotropic protons (two sets of double of doublet signals at $\delta_H = 3.56, 3.80$) coupled with each other and in turn with the vicinal propyl methine *HC*-1 (multiplet at $\delta_H = 4.07−4.14$). The latter coupled with the

dx.doi.org/10.1021/ci400723m | J. Chem. Inf. Model. 2014, 54, 1103−1116

Scheme 2. Reactions of 2-Bromo-3-pyridinecarbonitriles with Amines

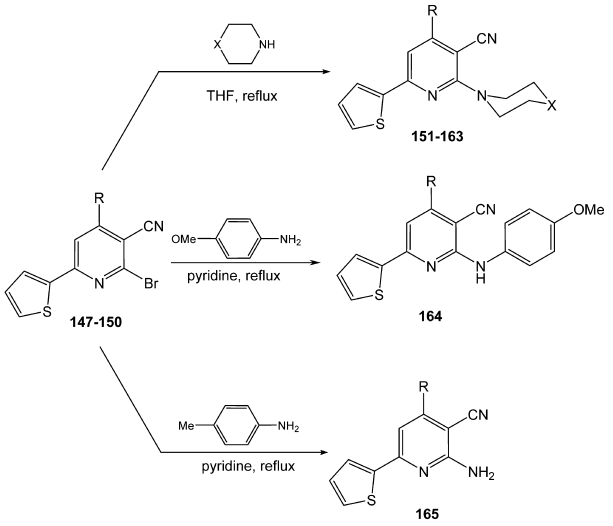

151; R = 4-ClC$_6$H$_4$, X = CH$_2$
152; R = 4-FC$_6$H$_4$, X = CH$_2$
153; R = 4-H$_3$CC$_6$H$_4$, X = CH$_2$
154; R = 2-thienyl, X = CH$_2$
155; R = 4-ClC$_6$H$_4$, X = O
156; R = 4-FC$_6$H$_4$, X = O
157; R = 4-H$_3$CC$_6$H$_4$, X = O
158; R = 2-thienyl, X = O
159; R = 4-ClC$_6$H$_4$, X = NMe
160; R = 4-ClC$_6$H$_4$, X = NEt
161; R = 4-FC$_6$H$_4$, X = NMe
162; R = 4-H$_3$CC$_6$H$_4$, X = NMe
163; R = 2-thienyl, X = NMe
164, **165**; R = 2-thienyl

vicinal propanedinitrile methine proton that appeared as a doublet at δ_H = 5.26 (Scheme 1).

Bromination of **143**−**146** in glacial acetic acid at 60−70 °C afforded ethyl 2-bromo-4,6-diaryl-3-pyridinecarbonitriles **147**−**150** in good yields (70−78%). The structures of **147**−**150** were inferred from spectroscopic (IR, ^{1}H NMR, ^{13}C NMR) and elemental analysis data. The IR spectra of **147**, as a representative example of this family, lacked any band assignable to a carbonyl function. However, a strong nitrile stretching vibration band was observed (ν = 2220 cm^{-1}). ^{1}H NMR spectra of **147** showed the characteristic pyridinyl *H*-5 as a singlet signal at δ_H = 8.20. ^{13}C NMR spectrum of **147** showed the pyridinyl quaternary *C*-3 and methine *HC*-5 at δ_C = 109.2, 116.9, respectively. Additionally, the nitrile carbon was observed at δ_C = 118.4 (Scheme 1).

Reaction of 2-bromo-3-pyridinecarbonitriles **147**−**150** with secondary amines (piperidine, morpholine, 1-methylpiperazine, and 1-ethylpiperazine) in refluxing tetrahydrofuran led to aromatic nucleophilic substitution affording 2-(alicyclic-amino)-3-pyridinecarbonitriles **151**−**163** in good yields (79−97%), whose structures were deduced through spectroscopic (IR, ^{1}H NMR, ^{13}C NMR) and elemental analysis data (Scheme 2). The ^{1}H NMR spectrum of **151**, as a representative example of this family, revealed the piperidinyl function as a multiplet signal at δ_H = 1.70−1.78 (piperidinyl H_2C-3, H_2C-4 and H_2C-5) beside a triplet signal at δ_H = 3.78 (piperidinyl H_2C-2 and H_2C-6). The morpholinyl function of **155** appeared in its ^{1}H NMR spectrum as two triplet signals at δ_H = 3.80, 3.90 assigned to morpholinyl CH_2N-3/5 and CH_2O-2/6, respectively. However, the 1-(4-methylpiperazinyl) residue of **159** was observed in its ^{1}H NMR spectrum as two triplet signals at δ_H = 2.69 and 3.88 beside a singlet signal at δ_H = 2.43 due to the piperazinyl methyl group. ^{13}C NMR spectrum of **153** exhibited the piperidinyl *C*-4, *C*-3/5, and *C*-2/6 at δ_C = 24.5, 25.9, and 50.1, respectively. The ^{13}C NMR spectrum of **155** revealed the morpholinyl CH_2N-3/5 and CH_2O-2/6 at δ_C = 49.3 and 66.4, respectively. The ^{13}C NMR spectrum of **159** revealed the piperazinyl *C*-2/6 and *C*-3/5 at δ_C = 48.7 and 54.8, respectively. For additional spectral data, see the Experimental Section.

Reaction of **150** with *p*-anisidine in refluxing pyridine afforded the expected 4,6-bis(2-thienyl)-2-[(4-methoxyphenyl)amino]-3-pyridinecarbonitrile (**164**). However, reaction of **150** with *p*-toluidine under the same conditions gave 2-amino-4,6-bis(2-thienyl)-3-pyridinecarbonitrile (**165**). Although formation of the latter product is unexpected however, similar observations describing this behavior were reported[6a−c,34−36] (Scheme 2).

VASODILATION PROPERTIES

Vasodilation properties of 3-pyridinecarbonitriles **147**−**165** were investigated in vitro using isolated thoracic aortic rings of rats precontracted with norepinephrine hydrochloride standard reported procedure[6a,c−e,21] and compared with prazosin hydrochloride (highly selective α_1-adrenoceptor antagonist), which was used as a reference standard. The observed data (Table 4 and Figures 1 and 2 of Supporting Information) reveal that all the synthesized compounds exhibited significant vasodilation properties compatible with the used standard reference. Additionally, compounds **147**, **153**, and **154** exhibit remarkable activity (IC_{50}, concentration necessary for 50% reduction of maximal norepinephrine hydrochloride induced contracture = 0.066, 0.084, and 0.045 mM, respectively), compared to prazosin hydrochloride, the used reference standard in the present study revealed a potency, IC_{50} = 0.487 mM.[37]

It was noticed that in most cases (compound **159** is an exception) substituting the pyridinecarbonitriles position-4 with a 4-(chlorophenyl) function enhanced the pharmacological properties relative to the 4-(fluorophenyl) analogue. In most cases (compound **152** is an exception) substitution at position-2 of the pyridinecarbonitrile nucleus with a piperidinyl function, enhanced the vasodilation activity compared to a morpholinyl residue.

EXPERIMENTAL SECTION

General Information Concerning Synthetic Methods. Melting points were determined on an Electrothermal Stuart SMP3 melting point apparatus. IR spectra (KBr) were recorded on a Shimadzu FT-IR 8400S spectrophotometer. ^{1}H NMR spectra were recorded on a Varian MERCURY 300 (^{1}H: 300 MHz) spectrometer. ^{13}C NMR spectra were recorded on a JEOL AS 500 (^{13}C: 125 MHz) spectrometer. The starting compounds **139**−**142**[40,38,39] were prepared according to previously reported procedures.

*Synthesis of (1,3-Diaryl-3-oxo-propyl)propanedinitriles **143**−**146** (General Procedure).* A mixture of equimolar amounts of appropriate **139**−**142** and malononitrile (10 mmol) in absolute ethanol (20 mL) containing morpholine (3−5 drops) was stirred at room temperature (20−25 °C) for 6 h. The solid which separated after storing the reaction mixture overnight at room temperature was collected and crystallized from a suitable solvent to afford **143**−**146**.

*[3-(4-Chlorophenyl-1-(2-thienyl)-3-oxo-propyl)-propanedinitrile (**143**).* Colorless microcrystals from *n*-butanol. Mp 152−154 °C (1.40 g, 89% yield). IR: ν 2260, 1653, 1516, 1491. ^{1}H NMR (DMSO-d_6): δ 3.56 (dd, *J* = 17.6, 5.6 Hz, 1H),

dx.doi.org/10.1021/ci400723m | J. Chem. Inf. Model. 2014, 54, 1103−1116

3.80 (dd, J = 17.4, 9.0 Hz, 1H), 4.07−4.14 (m, 1H), 5.26 (d, J = 6.6 Hz, 1H), 7.26 (dd, J = 5.1, 3.9 Hz, 1H), 7.46 (d, J = 9.0 Hz, 2H), 7.51 (d, J = 8.7 Hz, 2H), 8.02 (dd, J = 5.0, 1.1 Hz, 1H), 8.08 (dd, J = 3.9, 1.2 Hz, 1H). Anal. calcd for $C_{16}H_{11}ClN_2OS$: C, 61.05; H, 3.52; N, 8.90. Found: C, 61.18; H, 3.59; N, 9.13.

*[3-(4-Fluorophenyl-3-oxo-1-(2-thienyl)-propyl)-propanedinitrile (**144**).* Colorless microcrystals from methanol. Mp 160−162 °C (1.20 g, 81% yield). IR: ν 2261, 1651, 1605, 1510. ^{1}H NMR (DMSO-d_6): δ 3.56 (dd, J = 17.4, 5.7 Hz, 1H), 3.79 (dd, J = 17.4, 8.7 Hz, 1H), 4.07−4.14 (m, 1H), 5.25 (d, J = 6.3 Hz, 1H), 7.19−7.27 (m, 3H), 7.53 (dd, J = 8.6, 5.6 Hz, 2H), 8.02 (dd, J = 4.8, 0.9 Hz, 1H), 8.08 (dd, J = 3.9, 1.2 Hz, 1H). Anal. Calcd for $C_{16}H_{11}FN_2OS$: C, 64.42; H, 3.72; N, 9.39. Found: C, 64.58; H, 3.76; N, 9.48.

*[3-(4-Methylphenyl-3-oxo-1-(2-thienyl)-propyl)-propanedinitrile (**145**).* Colorless microcrystals from n-butanol. Mp 154−156 °C (1.30 g, 88% yield). IR: ν 2261, 1655, 1518, 1410. ^{1}H NMR ($CDCl_3$): δ 2.38 (s, 3H), 3.56 (dd, J = 18.0, 5.7 Hz, 1H), 3.64 (dd, J = 18.2, 8.6 Hz, 1H), 3.88−3.94 (m, 1H), 4.62 (d, J = 5.1 Hz, 1H), 7.17 (dd, J = 5.0, 3.8 Hz, 1H), 7.24 (d, J = 8.4 Hz, 2H), 7.34 (d, J = 8.4 Hz, 2H), 7.72 (dd, J = 5.0, 1.1 Hz, 1H), 7.79 (dd, J = 3.8, 1.1 Hz, 1H). Anal. Calcd for $C_{17}H_{14}N_2OS$: C, 69.36; H, 4.79; N, 9.52. Found: C, 69.41; H, 4.83; N, 9.61.

*[1,3-Bis(2-thienyl)-3-oxo-propyl)propanedinitrile (**146**).* Colorless microcrystals from benzene−light petroleum (60−80 °C) as 2:1 v/v. Mp 123−125 °C[39] (1.25 g, 87% yield).

*Synthesis of 2-Bromo-4,6-diaryl-3-pyridinecarbonitriles **147**−**150** (General Procedure).* To a solution of **143**−**146** (5 mmol) in glacial acetic acid (10 mL) at 60−70 °C, a solution of bromine (5.5 mmol) in glacial acetic acid (5 mL) was added dropwise with stirring over a period of 10 min. After complete addition, the reaction was kept at the same temperature for 3 h and stored at room temperature (20−25 °C) overnight. The separated solid was collected, washed with water, and crystallized from a suitable solvent to afford **147**−**150**.

*2-Bromo-4-(4-chlorophenyl)-6-(2-thienyl)-3-pyridinecarbonitrile (**147**).* Pale-yellow microcrystals from n-butanol. Mp 222−224 °C (1.35 g, 72% yield). IR: ν 2220, 1576, 1566. ^{1}H NMR (DMSO-d_6): δ 7.26 (t, J = 4.5 Hz, 1H), 7.69 (d, J = 8.7 Hz, 2H), 7.78 (d, J = 8.4 Hz, 2H), 7.90 (d, J = 4.8 Hz, 1H), 8.16 (d, J = 4.5 Hz, 1H), 8.20 (s, 1H). ^{13}C NMR (DMSO-d_6): δ 109.2, 116.9, 118.4, 129.4, 129.8, 130.6, 131.2, 133.2, 134.4, 136.0, 141.5, 144.7, 155.0, 155.4. Anal. Calcd for $C_{16}H_8BrClN_2S$: C, 51.16; H, 2.15; N, 7.46. Found: C, 51.21; H, 2.19; N, 7.58.

*2-Bromo-4-(4-fluorophenyl)-6-(2-thienyl)-3-pyridinecarbonitrile (**148**).* Yellow microcrystals from acetic acid. Mp 212−214 °C (1.40 g, 78% yield). IR: ν 2226, 1580, 1564. ^{1}H NMR (DMSO-d_6): δ 7.26 (dd, J = 5.0, 3.8 Hz, 1H), 7.46 (t, J = 9.0 Hz, 2H), 7.82 (dd, J = 9.0, 5.4 Hz, 2H), 7.90 (dd, J = 5.1, 1.2 Hz, 1H), 8.16 (dd, J = 3.9, 1.2 Hz, 1H), 8.20 (s, 1H). Anal. Calcd for $C_{16}H_8BrFN_2S$: C, 53.50; H, 2.24; N, 7.80. Found: C, 53.62; H, 2.27; N, 7.78.

*2-Bromo-4-(4-methylphenyl)-6-(2-thienyl)-3-pyridinecarbonitrile (**149**).* Almost colorless microcrystals from acetic acid. Mp 228−230 °C (1.25 g, 70% yield). IR: ν 2220, 1584, 1516; ^{1}H NMR (DMSO-d_6): δ 2.42 (s, 3H), 7.25 (t, J = 5.1 Hz, 1H), 7.41 (d, J = 7.8 Hz, 2H), 7.64 (d, J = 8.1 Hz, 2H), 7.89 (dd, J = 5.0, 1.1 Hz, 1H), 8.15 (s, 1H), 8.16 (dd, J = 5.0, 1.4 Hz, 1H). Anal. Calcd for $C_{17}H_{11}BrN_2S$: C, 57.48; H, 3.12; N, 7.89. Found: C, 57.39; H, 3.18; N, 7.97.

*2-Bromo-4,6-bis(2-thienyl)-3-pyridinecarbonitrile (**150**).* Colorless microcrystals from n-butanol. Mp 181−183 °C (1.30 g, 75% yield). IR: ν 2222, 1574, 1501. ^{1}H NMR ($CDCl_3$): δ 7.17−7.27 (m, 2H), 7.57−7.63 (m, 2H), 7.72 (s, 1H), 7.79 (d, J = 3.9 Hz, 1H), 7.95 (d, J = 3.9 Hz, 1H). Anal. Calcd for $C_{14}H_7BrN_2S_2$: C, 48.42; H, 2.03; N, 8.07. Found: C, 48.53; H, 2.01; N, 8.19.

*Reaction of **147**−**150** with Secondary Amines (General Procedure).* A mixture of **147**−**150** (5 mmol) and the corresponding secondary amine (10 mmol) in tetrahydrofuran (20 mL) was heated under reflux for the specified times. The reaction mixture was evaporated to dryness, and the residue was triturated material with methanol (5 mL), collected, and crystallized from a suitable solvent to afford **151**−**163**.

*4-(4-Chlorophenyl)-2-(1-piperidinyl)-6-(2-thienyl)-3-pyridinecarbonitrile (**151**).* Reaction time 7 h. Yellow microcrystals from n-butanol. Mp 152−154 °C (1.85 g, 97% yield). IR: ν 2201, 1593, 1566. ^{1}H NMR ($CDCl_3$): δ 1.68−1.80 (m, 6H), 3.78 (t, J = 4.8 Hz, 4H), 7.06 (s, 1H), 7.13 (dd, J = 4.8, 3.9 Hz, 1H), 7.45−7.57 (m, 5H), 7.66 (d, J = 3.9 Hz, 1H). Anal. Calcd for $C_{21}H_{18}ClN_3S$: C, 66.39; H, 4.78; N, 11.06. Found: C, 66.47; H, 4.86; N, 11.18.

*4-(4-Fluorophenyl)-2-(1-piperidinyl)-6-(2-thienyl)-3-pyridinecarbonitrile (**152**).* Reaction time 6 h. Pale-yellow microcrystals from ethanol. Mp 125−127 °C (1.60 g, 88% yield). IR: ν 2208, 1605, 1572. ^{1}H NMR ($CDCl_3$): δ 1.64−1.82 (m, 6H), 3.77 (t, J = 5.1 Hz, 4H), 7.07 (s, 1H), 7.13 (dd, J = 5.1, 3.9 Hz, 1H), 7.20 (t, J = 8.6 Hz, 2H), 7.48 (d, J = 5.1 Hz, 1H), 7.58 (dd, J = 8.4, 5.4 Hz, 2H), 7.67 (dd, J = 3.6, 0.9 Hz, 1H). Anal. Calcd for $C_{21}H_{18}FN_3S$: C, 69.40; H, 4.99; N, 11.56. Found: C, 69.52; H, 5.04; N, 11.69.

*4-(4-Methylphenyl)-2-(1-piperidinyl)-6-(2-thienyl)-3-pyridinecarbonitrile (**153**).* Reaction time 7 h. Pale-yellow microcrystals from n-butanol. Mp 139−141 °C (1.55 g, 86% yield). IR: ν 2201, 1566, 1533. ^{1}H NMR ($CDCl_3$): δ 1.70−1.81 (m, 6H), 2.44 (s, 3H), 3.76 (t, J = 5.1 Hz, 4H), 7.11 (s, 1H), 7.13 (dd, J = 5.1, 3.6 Hz, 1H), 7.32 (d, J = 7.8 Hz, 2H), 7.46 (dd, J = 5.0, 0.8 Hz, 1H), 7.50 (d, J = 8.1 Hz, 2H), 7.67 (dd, J = 3.6, 0.9 Hz, 1H). ^{13}C NMR (DMSO-d_6): δ 21.4, 24.5, 25.9, 50.1, 91.5, 109.9, 118.5, 128.4, 129.3, 129.8, 131.1, 134.5, 140.1, 144.2, 153.2, 157.1, 162.7. Anal. Calcd for $C_{22}H_{21}N_3S$: C, 73.50; H, 5.89; N, 11.69. Found: C, 73.58; H, 5.91; N, 11.77.

*4,6-Bis(2-thienyl)-2-(1-piperidinyl)-3-pyridinecarbonitrile (**154**).* Reaction time 7 h. Pale-yellow microcrystals from n-butanol. Mp 106−108 °C (1.60 g, 91% yield). IR: ν 2207, 1574, 1539. ^{1}H NMR ($CDCl_3$): δ 1.60−1.90 (m, 6H), 3.75 (t, J = 5.0 Hz, 4H), 7.14 (dd, J = 5.0, 3.8 Hz, 1H), 7.20 (dd, J = 5.0, 3.8 Hz, 1H), 7.21 (s, 1H), 7.48 (dd, J = 5.0, 1.1 Hz, 1H), 7.52 (dd, J = 5.0, 1.1 Hz, 1H), 7.69 (dd, J = 3.8, 1.1 Hz, 1H), 7.78 (dd, J = 3.6, 1.2 Hz, 1H). ^{13}C NMR (DMSO-d_6): δ 24.5, 25.9, 50.2, 89.7, 108.9, 118.7, 128.6, 128.9, 129.3, 130.5, 130.6, 131.4, 138.0, 143.9, 148.7, 153.4, 163.2. Anal. Calcd for $C_{19}H_{17}N_3S_2$: C, 64.93; H, 4.88; N, 11.95. Found: C, 64.98; H, 4.93; N, 12.11.

*4-(4-Chlorophenyl)-2-(4-morpholinyl)-6-(2-thienyl)-3-pyridinecarbonitrile (**155**).* Reaction time 5 h. Yellow microcrystals from n-butanol. Mp 185−187 °C (1.75 g, 92% yield). IR: ν 2203, 1595, 1572. ^{1}H NMR ($CDCl_3$): δ 3.80 (t, J = 4.4 Hz, 4H), 3.90 (t, J = 4.5 Hz, 4H), 7.13−7.16 (m, 2H), 7.48−7.55 (m, 5H), 7.68 (d, J = 3.6 Hz, 1H). ^{13}C NMR (DMSO-d_6): δ 49.3, 66.4, 91.8, 110.7, 118.1, 128.8, 129.25, 129.3, 131.2, 131.4, 135.4, 135.9, 143.8, 153.4, 155.8, 162.1. Anal. Calcd for $C_{20}H_{16}ClN_3OS$: C, 62.90; H, 4.22; N, 11.00. Found: C, 62.98; H, 4.20; N, 11.12.

*4-(4-Fluorophenyl)-2-(4-morpholinyl)-6-(2-thienyl)-3-pyridinecarbonitrile (**156**).* Reaction time 5 h. Yellow microcrystals from n-butanol. Mp 191−193 °C (1.65 g, 90% yield). IR: ν 2199, 1603, 1560. ^{1}H NMR ($CDCl_3$): δ 3.80 (t, J = 4.2 Hz, 4H), 3.91 (t,

dx.doi.org/10.1021/ci400723m | J. Chem. Inf. Model. 2014, 54, 1103−1116

J = 4.2 Hz, 4H), 7.15 (dd, J = 5.1, 4.2 Hz, 1H), 7.16 (s, 1H), 7.22 (t, J = 8.6 Hz, 2H), 7.50 (dd, J = 5.1, 0.6 Hz, 1H), 7.56−7.61 (m, 2H), 7.68 (dd, J = 3.6, 0.9 Hz, 1H). ^{13}C NMR (DMSO-d_6): δ 49.3, 66.4, 92.0, 110.8, 116.1, 116.3, 118.2, 128.8, 129.3, 131.4, 131.7, 131.8, 133.5, 143.8, 153.4, 156.0, 162.2, 162.6, 164.6. Anal. Calcd for $C_{20}H_{16}FN_3OS$: C, 65.74; H, 4.41; N, 11.50. Found: C, 65.79; H, 4.47; N, 11.62.

*4-(4-Methylphenyl)-2-(4-morpholinyl)-6-(2-thienyl)-3-pyridinecarbonitrile (**157**).* Reaction time 6 h. Yellow microcrystals from *n*-butanol. Mp 198−200 °C (1.65 g, 91% yield). IR: ν 2197, 1560, 1533. ^{1}H NMR ($CDCl_3$): δ 2.45 (s, 3H), 3.79 (t, J = 4.4 Hz, 4H), 3.91 (t, J = 4.5 Hz, 4H), 7.14 (t, J = 4.4 Hz, 1H), 7.19 (s, 1H), 7.33 (d, J = 7.8 Hz, 2H), 7.46−7.52 (m, 3H), 7.67 (d, J = 3.6 Hz, 1H). ^{13}C NMR (DMSO-d_6): δ 21.4, 49.4, 66.5, 92.1, 110.7, 118.3, 128.6, 129.3, 129.8, 131.3, 134.2, 140.2, 143.9, 153.3, 157.1, 162.4. Anal. Calcd for $C_{21}H_{19}N_3OS$: C, 69.78; H, 5.30; N, 11.62. Found: C, 69.85; H, 5.34; N, 11.68.

*4,6-Bis(2-thienyl)-2-(4-morpholinyl)-3-pyridinecarbonitrile (**158**).* Reaction time 7 h. Yellow microcrystals from *n*-butanol. Mp 203−205 °C (1.55 g, 88% yield). IR: ν 2199, 1560, 1541. ^{1}H NMR ($CDCl_3$): δ 3.66 (t, J = 4.5 Hz, 4H), 3.78 (t, J = 4.5 Hz, 4H), 7.22 (dd, J = 5.0, 3.8 Hz, 1H), 7.30 (dd, J = 5.0, 3.8 Hz, 1H), 7.60 (s, 1H), 7.78 (dd, J = 5.0, 1.1 Hz, 1H), 7.85 (dd, J = 3.6, 1.2 Hz, 1H), 7.91 (dd, J = 5.3, 1.4 Hz, 1H), 8.05 (dd, J = 3.8, 1.1 Hz, 1H). Anal. Calcd for $C_{18}H_{15}N_3OS_2$: C, 61.17; H, 4.28; N, 11.89. Found: C, 61.30; H, 4.34; N, 12.03.

*4-(4-Chlorophenyl)-2-[1-(4-methylpiperazinyl)]-6-(2-thienyl)-3-pyridinecarbonitrile (**159**).* Reaction time 10 h. Pale-yellow microcrystals from n-butanol. Mp 184−186 °C (1.60 g, 81% yield). IR: ν 2208, 1595, 1574. ^{1}HNMR ($CDCl_3$): δ 2.43 (s, 3H), 2.69 (t, J = 4.5 Hz, 4H), 3.88 (t, J = 5.0 Hz, 4H), 7.12 (s, 1H), 7.14 (t, J = 4.4 Hz, 1H), 7.40−7.55 (m, 5H), 7.67 (dd, J = 3.8, 1.1 Hz, 1H). ^{13}CNMR (DMSO-d_6): δ 46.2, 48.7, 54.8, 91.6, 110.3, 118.2, 128.7, 129.25, 129.3, 131.3, 131.4, 135.3, 136.0, 143.9, 153.4, 155.8, 162.1. Anal. Calcd for $C_{21}H_{19}ClN_4S$: C, 63.87; H, 4.85; N, 14.19. Found: C, 64.02; H, 4.93; N, 14.27.

*4-(4-Chlorophenyl)-2-[1-(4-ethylpiperazinyl)]-6-(2-thienyl)-3-pyridinecarbonitrile (**160**).* Reaction time 12 h. Yellow microcrystals from *n*-butanol. Mp 167−169 °C (1.75 g, 86% yield). IR: ν 2212, 1597, 1574. ^{1}H NMR ($CDCl_3$): δ 1.22 (t, J = 7.2 Hz, 3H), 2.62 (q, J = 7.2 Hz, 2H), 2.62−2.82 (m, 4H), 3.91 (t, J = 4.7 Hz, 4H), 7.12 (s, 1H), 7.14 (t, J = 4.8 Hz, 1H), 7.48−7.55 (m, 5H), 7.67 (d, J = 3.9 Hz, 1H). ^{13}C NMR (DMSO-d_6): δ 12.4, 48.8, 52.1, 52.6, 91.5, 110.3, 118.2, 128.8, 129.3, 129.4, 131.3, 131.4, 135.3, 136.1, 143.9, 153.4, 155.9, 162.0. Anal. Calcd for $C_{22}H_{21}ClN_4S$: C, 64.61; H, 5.18; N, 13.70. Found: C, 64.73; H, 5.16; N, 13.79.

*4-(4-Fluorophenyl)-2-[1-(4-methylpiperazinyl)]-6-(2-thienyl)-3-pyridinecarbonitrile (**161**).* Reaction time 10 h. Yellow microcrystals from ethanol. Mp 158−159 °C (1.50 g, 79% yield). IR: ν 2210, 1574, 1545. ^{1}H NMR ($CDCl_3$): δ 2.41 (s, 3H), 2.67 (t, J = 5.0 Hz, 4H), 3.87 (t, J = 5.1 Hz, 4H), 7.12 (s, 1H), 7.14 (dd, J = 5.1, 3.9 Hz, 1H), 7.18−7.24 (m, 2H), 7.49 (dd, J = 5.1, 1.2 Hz, 1H), 7.55−7.61 (m, 2H), 7.67 (dd, J = 3.8, 1.1 Hz, 1H). Anal. Calcd for $C_{21}H_{19}FN_4S$: C, 66.64; H, 5.06; N, 14.80. Found: C, 66.79; H, 5.13; N, 15.02.

*4-(4-Methylphenyl)-2-[1-(4-methylpiperazinyl)]-6-(2-thienyl)-3-pyridinecarbonitrile (**162**).* Reaction time 10 h. Pale-yellow microcrystals from methanol. Mp 151−153 °C (1.60 g, 86% yield). IR: ν 2212, 1575, 1535. ^{1}H NMR ($CDCl_3$): δ 2.43 (s, 3H), 2.44 (s, 3H), 2.70 (t, J = 4.8 Hz, 4H), 3.87 (t, J = 4.8 Hz, 4H), 7.13 (t, J = 4.4 Hz, 1H), 7.16 (s, 1H), 7.33 (d, J = 8.1 Hz, 2H), 7.47−7.51 (m, 3H), 7.66 (d, J = 3.9 Hz, 1H). ^{13}C NMR (DMSO-d_6): δ 21.4, 46.2, 48.8, 54.9, 91.8, 110.4, 118.4, 128.4, 128.6, 128.7, 128.9, 129.3, 129.8, 131.2, 134.3, 140.2, 144.0, 153.2, 157.1, 162.4. Anal. Calcd for $C_{22}H_{22}N_4S$: C, 70.56; H, 5.92; N, 14.96. Found: C, 70.71; H, 5.96; N, 14.88.

*4,6-Bis(2-thienyl)-2-[1-(4-methylpiperazinyl)]-3-pyridinecarbonitrile (**163**).* Reaction time 12 h. Yellow microcrystals from methanol. Mp 128−130 °C (1.50 g, 82% yield). IR: ν 2205, 1574, 1543. ^{1}H NMR ($CDCl_3$): δ 2.4 (s, 3H), 2.65 (t, J = 5.0 Hz, 4H), 3.83 (t, J = 5.0 Hz, 4H), 7.14 (dd, J = 5.1, 3.6 Hz, 1H), 7.20 (dd, J = 5.1, 3.6 Hz, 1H), 7.25 (s, 1H), 7.48 (dd, J = 5.1, 1.2 Hz, 1H), 7.52 (dd, J = 5.1, 1.2 Hz, 1H), 7.68 (dd, J = 3.8, 1.1 Hz, 1H), 7.77 (dd, J = 3.8, 1.1 Hz, 1H). ^{13}C NMR (DMSO-d_6): δ 46.2, 48.9, 54.9, 90.0, 109.4, 118.5, 128.7, 128.9, 129.3, 130.5, 130.6, 131.4, 137.9, 143.7, 148.7, 153.4, 162.9. Anal. Calcd for $C_{19}H_{18}N_4S_2$: C, 62.27; H, 4.95; N, 15.29. Found: C, 62.34; H, 4.98; N, 15.37.

*Reaction of **150** with Primary Amines (General Procedure).* A mixture of **150** (5 mmol) and the corresponding primary amine (5.5 mmol) in pyridine (20 mL) was heated under reflux for the appropriate time. The solid that separated on pouring the reaction mixture into ice-cold water (200 mL) and acidification with dil. HCl (5%) was collected, washed with water, and purified by silica gel TLC (F_{254}) affording **164** and **165**.

*4,6-Bis(2-thienyl)-2-[(4-methoxyphenyl)amino]-3-pyridinecarbonitrile (**164**).* Obtained via reaction of **150** and *p*-anisidine. Reaction time 15 h. Yellow microcrystals purified by silica gel TLC (F_{254}) using methylene chloride−light petroleum (60−80 °C) as 1:2 v/v for elution. Mp 197−199 °C (1.10 g, 57% yield). IR: ν 3325, 2210, 1601, 1578. ^{1}H NMR ($CDCl_3$): δ 3.86 (s, 3H), 6.97 (d, J = 9.3 Hz, 2H), 7.15 (t, J = 4.5 Hz, 1H), 7.22 (d, J = 5.1 Hz, 1H), 7.24 (s, 1H), 7.50 (d, J = 5.1 Hz, 1H), 7.56 (d, J = 5.1 Hz, 1H), 7.61 (d, J = 8.7 Hz, 2H), 7.73 (br s, 1H), 7.86 (d, J = 4.5 Hz, 1H). ^{13}C NMR (DMSO-d_6): δ 55.7, 87.0, 108.3, 114.0, 117.6, 123.8, 128.5, 128.9, 129.3, 130.2, 130.6, 131.5, 133.0, 137.9, 144.0, 147.6, 153.8, 155.8, 157.6. Anal. Calcd for $C_{21}H_{15}N_3OS_2$: C, 64.76; H, 3.88; N, 10.79. Found: C, 64.88; H, 3.94; N, 10.92.

*2-Amino-4,6-bis(2-thienyl)-3-pyridinecarbonitrile (**165**).* Obtained via reaction of **150** and *p*-toluidine. Reaction time 18 h. Pale-yellow microcrystals purified by silica gel TLC (F_{254}) using methylene chloride−light petroleum (60−80 °C) as 1:2 v/v for elution. Mp 177−179 °C (0.75 g, 53% yield). IR: ν 3478, 3370, 2210, 1626, 1572. ^{1}H NMR (DMSO-d_6): δ 6.99 (br s, 2H), 7.19 (dd, J = 5.3, 3.8 Hz, 1H), 7.28 (dd, J = 5.1, 3.6 Hz, 1H), 7.36 (s, 1H), 7.74 (dd, J = 5.0, 1.1 Hz, 1H), 7.84 (dd, J = 3.8, 1.1 Hz, 1H), 7.87 (dd, J = 5.1, 1.2 Hz, 1H), 7.98 (dd, J = 3.8, 1.1 Hz, 1H). ^{13}C NMR (DMSO-d_6): δ 84.5, 106.8, 117.9, 128.4, 128.9, 129.2, 129.8, 130.2, 131.0, 138.1, 143.8, 146.8, 154.8, 161.7. Anal. Calcd for $C_{14}H_9N_3S_2$: C, 59.34; H, 3.20; N, 14.83. Found: C, 59.51; H, 3.18; N, 15.04.

Vasodilation Activity Screening. The vasodilation activity screening procedure was carried out according to the standard reported in vitro bioassay technique[6a,c−e,21] by testing the effects of the synthesized compounds on isolated thoracic aortic rings of male Wistar rats (250−350 g) precontracted with norepinephrine hydrochloride. After light ether anesthesia, the rats were sacrificed by cervical dislocation. The aortae were immediately excised, freed of extraneous tissues, and prepared for isometric tension recording. Aorta was cut into (3−5 mm width) rings and each ring was placed in a vertical chamber "10 mL jacketed automatic multi-chamber organ bath system (Model no. ML870B6/C, Panlab, Spain)" filled with Krebs solution composed of (in mM): NaCl, 118.0; KCl, 4.7; $NaHCO_3$, 25.0;

$CaCl_2$, 1.8; NaH_2PO_4, 1.2; $MgSO_4$, 1.2; glucose, 11.0 and oxygenated with carbogen gas (95% O_2/5% CO_2) at 37 ± 0.5 °C. Each aortic ring was mounted between two stainless steel hooks passed through its lumen. The lower hook was fixed between two plates, while the upper one was attached to a force displacement transducer (Model no. MLT0201, Panlab, Spain) connected to an amplifier (PowerLab, AD Instruments Pty. Ltd.), which was connected to a computer. The Chart for windows (v 3.4) software was used to record and elaborate data.

Preparations were stabilized under 2 g resting tension during 2 h, and then the contracture response to norepinephrine hydrochloride (10^{-6} M) was measured before and after exposure to increasing concentrations of the tested synthesized compounds. The tested compounds were dissolved in dimethylsulfoxide (DMSO) as stock solution (10 mL of 0.005 M). Control experiments were performed in the presence of DMSO alone, at the same concentrations as those used with the derivatives tested, which demonstrated that the solvent did not affect the contractile response of isolated aorta. The observed vasodilation activity screening data for the newly synthesized compounds are expressed as IC_{50}, concentration necessary for 50% reduction of maximal norepinephrine hydrochloride induced contracture.

CONCLUSIONS

A highly representative and diverse data set of seven vasodilatory chemical classes analyzed with molecular field topology analysis resulted in a statistically significant relationship between the structure and the title activity. Based on this model, predictions for 19 newly synthesized compounds were made, which were subsequently biotested and demonstrated high vasodilatory potency. This QSAR model was also used for topological functional core identification. Such a functional core can be a valuable tool in the design of antihypertensive drugs with more than one mechanism of action.

ASSOCIATED CONTENT

Supporting Information

Charts represent the effect of synthesized compounds **147**−**165** on contracture induced by norepinephrine hydrochloride (NE·HCl) in rat thoracic aortic rings and the potency. This material is available free of charge via the Internet at http://pubs.acs.org

AUTHOR INFORMATION

Corresponding Author

*E-mail: charlesdennishall@gmail.com.

Notes

The authors declare no competing financial interest.

○Deceased

ACKNOWLEDGMENTS

This study was supported financially by the Science and Technology Development Fund (STDF), Egypt, grant no. 1357.

ABBREVIATIONS

MFTA, molecular field topology analysis; MSG, molecular super graph

REFERENCES

(1) Kearney, P. M.; Whelton, M.; Reynolds, K.; Muntner, P.; Whelton, P. K.; He, J. Global Burden of Hypertension: Analysis of Worldwide Data. *Lancet* **2005**, *365*, 217−223.

(2) Burt, V. L.; Cutler, J. A.; Higgins, M.; Horan, M. J.; Labarthe, D.; Whelton, P.; Brown, C.; Roccella, E. J. Trends in the Prevalence, Awareness, Treatment, and Control of Hypertension in the Adult US Population: Data from the Health Examination Surveys, 1960 to 1991. *Hypertension* **1995**, *26*, 60−69.

(3) Egan, B. M.; Zhao, Y.; Axon, R. N. US Trends in Prevalence, Awareness, Treatment, and Control of Hypertension, 1988−2008. *JAMA, J. Am. Med. Assoc.* **2010**, *303*, 2043−2050.

(4) McInnes, G. T. *Clinical Pharmacology and Therapeutics of Hypertension*; Elsevier: Amsterdam, The Netherlands, 2008.

(5) Klabunde, R. E. *Cardiovascular Physiology Concepts*; Lippincott Williams & Wilkins: Philadelphia, PA, 2004.

(6) (a) Girgis, A. S.; Kalmouch, A.; Ellithey, M. Synthesis of Novel Vasodilatory Active Nicotinate Esters with Amino Acid Function. *Bioorg. Med. Chem.* **2006**, *14*, 8488−8494. (b) Girgis, A. S.; Hosni, H. M.; Barsoum, F. F. Novel Synthesis of Nicotinamide Derivatieves of Cytotoxic Properties. *Bioorg. Med. Chem.* **2006**, *14*, 4466−4476. (c) Girgis, A. S.; Mishriky, N.; Farag, A. M.; El-Eraky, W. I.; Farag, H. Synthesis of New 3-Pyridinecarboxylates of Potential Vasodilation Properties. *Eur. J. Med. Chem.* **2008**, *43*, 1818−1827. (d) Girgis, A. S.; Ismail, N. S. M.; Farag, H. Facile Synthesis, Vasorelaxant Properties and Molecular Modeling Studies of 2-Amino-8*a*-methoxy-4*H*-pyrano[3,2-*c*]pyridine-3-carbonitriles. *Eur. J. Med. Chem.* **2011**, *46*, 2397−2407. (e) Girgis, A. S.; Ismail, N. S. M.; Farag, H.; El-Eraky, W. I.; Saleh, D. O.; Tala, S. R.; Katritzky, A. R. Regioselective Synthesis and Molecular Modelling Study of Vasorelaxant Active 7,9-Dioxa-1,2-diaza-spiro[4,5]-dec-2-ene-6,10-diones. *Eur. J. Med. Chem.* **2010**, *45*, 4229−4238.

(7) Badawneh, M.; Ferrarini, P. L.; Calderone, V.; Manera, C.; Martinotti, E.; Mori, C.; Saccomanni, G.; Testai, L. Synthesis and Evaluation of Antihypertensive Activity of 1,8-Naphthyridine Derivatives. Part X. *Eur. J. Med. Chem.* **2001**, *36*, 925−934.

(8) Quezada, E.; Delogu, G.; Picciau, C.; Santana, L.; Podda, G.; Borges, F.; García-Morales, V.; Viña, D.; Orallo, F. Synthesis and Vasorelaxant and Platelet Antiaggregatory Activities of a New Series of 6-Halo-3-phenylcoumarins. *Molecules* **2010**, *15*, 270−279.

(9) Bansal, R.; Kumar, D.; Carron, R.; de la Calle, C. Synthesis and Vasodilatory Activity of Some Amide Derivatives of 6-(4-Carboxymethyloxyphenyl)-4,5-dihydro-3(2H)-pyridazinone. *Eur. J. Med. Chem.* **2009**, *44*, 4441−4447.

(10) Silva, A. G.; Zapata-Sudo, G.; Kummerle, A. E.; Fraga, C. A. M.; Barreiro, E. J.; Sudo, R. T. Synthesis and Vasodilatory Activity of New N-Acetylhydrazone Derivatives, Designed as LASSBio-294 Analogues. *Bioorg. Med. Chem.* **2005**, *13*, 3431−3437.

(11) Campos-Toimil, M.; Orallo, F.; Santana, L.; Uriarte, E. Synthesis and Vasorelaxant Activity of New Coumarin and Furocoumarin Derivatives. *Bioorg. Med. Chem. Lett.* **2002**, *12*, 783−786.

(12) Chegaev, K.; Lazzarato, L.; Marcarino, P.; Di Stilo, A.; Fruttero, R.; Vanthuyne, N.; Roussel, C.; Gasco, A. Synthesis of Some Novel Organic Nitrates and Comparative in vitro Study of their Vasodilator Profile. *J. Med. Chem.* **2009**, *52*, 4020−4025.

(13) Vilar, S.; Quezada, E.; Alcaide, C.; Orallo, F.; Santana, L.; Uriarte, E. Quantitative Structure Vasodilatory Activity Relationship − Synthesis and "in silico" and "in vitro" Evaluation of Resveratrol-Coumarin Hybrids. *QSAR Comb. Sci.* **2007**, *26*, 317−332.

(14) Abouzid, K.; Hakeem, M. A.; Khalil, O.; Maklad, Y. Pyridazinone Derivatives: Design, Synthesis, and in vitro Vasorelaxant Activity. *Bioorg. Med. Chem.* **2008**, *16*, 382−389.

(15) Dong, X.; Wang, Y.; Liu, T.; Wu, P.; Gao, J.; Xu, J.; Yang, B.; Hu, Y. Flavonoids as Vasorelaxant Agents: Synthesis, Biological Evaluation and Quantitative Structure Activities Relationship (QSAR) Studies. *Molecules* **2011**, *16*, 8257−8272.

(16) (a) Palyulin, V. A.; Radchenko, E. V.; Zefirov, N. S. Molecular Field Topology Analysis Method in QSAR Studies of Organic Compounds. *J. Chem. Inf. Comput. Sci.* **2000**, *40*, 659−667. (b) Palyulin, V. A.; Zefirov, N. S. Generation of Molecular Graphs for QSAR Studies. *Dokl. Chem.* **2005**, *402*, 81−85.

(17) (a) Zhan, W.; Liang, Z.; Zhu, A.; Kurtkaya, S.; Shim, H.; Snyder, J. P.; Liotta, D. C. Discovery of Small Molecule CXCR4 Antagonists. *J. Med. Chem.* **2007**, *50*, 5655−5664. (b) Berhanu, W. M.; Pillai, G. G.;

Oliferenko, A. A.; Katrtitzky, A. R. Quantitative Structure−Activity/Property Relationships: The Ubiquitous Links Between Cause and Effect. *ChemPlusChem* **2012**, *77*, 507−517.
(18) Radchenko, E. V.; Makhaeva, G. F.; Malygin, V. V.; Sokolov, V. B.; Palyulin, V. A.; Zefirov, N. S. Modelling of the Relationships Between the Structure of o-Phosphorylated Oximes and their Anticholinesterase Activity and Selectivity Using Molecular Field Topology Analysis (MFTA). *Dokl. Biochem. Biophys.* **2008**, *418*, 47−51.
(19) Chupakhin, V. I.; Bobrov, S. V.; Radchenko, E. V.; Palyulin, V. A.; Zefirov, N. S. Computer-Aided Ddesign of Selective Ligands of the Benzodiazepine-Binding Site of the $GABA_A$ Receptor. *Dokl. Chem.* **2008**, *422*, 227−230.
(20) Girgis, A. S.; Farag, H.; Ismail, N. S. M.; George, R. F. Synthesis, Hypnotic Properties and Molecular Modelling Studies of 1,2,7,9-Tetraaza-spiro[4.5]dec-2-ene-6,8,10-triones. *Eur. J. Med. Chem.* **2011**, *46*, 4964−4969.
(21) Nofal, Z. M.; Srour, A. M.; El-Eraky, W. I.; Saleh, D. O.; Girgis, A. S. Rational Design, Synthesis and QSAR Study of Vasorelaxant Active 3-Pyridinecarbonitriles Incorporating 1*H*-Benzimidazol-2-yl Function. *Eur. J. Med. Chem.* **2013**, *63*, 14−21.
(22) Vilar, S.; Quezada, E.; Santana, L.; Uriarte, E.; Yánez, M.; Fraiz, N.; Alcaide, C.; Cano, E.; Orallo, F. Design, Synthesis, and Vasorelaxant and Platelet Antiaggregatory Activities of Coumarin-Resveratrol Hybrids. *Bioorg. Med. Chem. Lett.* **2006**, *16*, 257−261.
(23) Burns, D. M.; Ruddock, M. W.; Walker, M. D.; Allen, J. M.; Kennovin, G. D.; Hirst, D. G. Nicotinamide-Inhibited Vasoconstriction: Lack of Dependence on Agonist Signalling Pathways. *Eur. J. Pharmacol.* **1999**, *374*, 213−220.
(24) Eguchi, S.; Miyashita, S.; Kitamura, Y.; Kawasaki, H. $\alpha3\beta4$-Nicotinic Receptors Mediate Adrenergic Nerve- and Peptidergic (CGRP) Nerve-Dependent Vasodilation Induced by Nicotine in Rat Mesentergic Arteries. *Br. J. Pharmacol.* **2007**, *151*, 1216−1223.
(25) Si, M.; Lee, T. J. F. Presynaptic $\alpha7$-Nicotinic Acetylcholine Receptors Mediate Nicotine-Induced Nitric Oxidergic Neurogenic Vasodilation in Porcine Basilar Arteries. *J. Pharmacol. Exp. Ther.* **2001**, *298*, 122−128.
(26) Toba, H.; Nakagawa, Y.; Miki, S.; Shimizu, T.; Yoshimura, A.; Inoue, R.; Asayama, J.; Kobara, M.; Nakata, T. Calcium Channel Blockades Exhibit Anti-inflammatory and Antioxidative Effects by Augmentation of Endothelial Nitric Oxide Synthase and the Inhibition of Angiotensin Converting Enzyme in the *N*G-Nitro-L-arginine methyl ester - Induced Hypertensive Rat Aorta: Vasoprotective Effects Beyond the Blood Pressure-Lowering Effects of Amlodipine and Manidipine. *Hypertens. Res.* **2005**, *28*, 689−700.
(27) Clark, R. D.; Caroon, J. M.; Repke, D. B.; Strosberg, A. M.; Bitter, S. M.; Okada, M. D.; Michel, A. D.; Whiting, R. L. Antihypertensive 9-Substituted 1-Oxa-4,9-diazaspiro[5.5]undecan-3-ones. *J. Med. Chem.* **1983**, *26*, 855−861.
(28) Ferrarini, P. L.; Mori, C.; Calderone, V.; Calzolari, L.; Nieri, P.; Saccomanni, G.; Martinotti, E. Synthesis of 1,8-Naphthyridine Derivatives: Potential Antihypertensive Agents − Part VIII. *Eur. J. Med. Chem.* **1999**, *34*, 505−513.
(29) Silva, C. L. M.; Noël, F.; Barreiro, E. J. Cyclic GMP-Dependent Vasodilatory Properties of LASSBio-294 in Rat Aorta. *Br. J. Pharmacol.* **2002**, *135*, 293−298.
(30) Franke, R.; Huebel, S.; Streich, W. J. Substructural QSAR Approaches and Topological Pharmacophores. *Environ. Health Persp.* **1985**, *61*, 239−255.
(31) Schneider, G.; Neidhart, W.; Giller, T.; Schmid, G. Scaffold-Hopping" by Topological Pharmacophore Search: a Contribution to Virtual Screening. *Angew. Chem., Int. Ed.* **1999**, *38*, 2894−2896.
(32) Bonachera, F.; Parent, B.; Barbosa, F.; Froloff, N.; Horvath, D. Fuzzy Tricentric Pharmacophore Fingerprints. 1. Topological Fuzzy Pharmacophore Triplets and Adapted Molecular Similarity Scoring Schemes. *J. Chem. Inf. Model.* **2006**, *46*, 2457−2477.
(33) Horvath, D. *Topological pharmacophores, Ch. 2 in Chemo-informatics Approaches to Virtual Screening*; Varnek, A., Tropsha, A., Eds.; RSC: Cambridge, U.K., 2008.
(34) Girgis, A. S.; Hosni, H. M.; Barsoum, F. F.; Amer, A. M. M.; Farag, I. S. A. Novel Nicotinate Esters of Vasodilatation Activity. *Boll. Chim. Farm.* **2004**, *143*, 365−375.
(35) Girgis, A. S.; Kalmouch, A.; Hosni, H. M. Synthesis of Novel 3-Pyridinecarbonitriles with Amino Acid Function and their Fluorescence Properties. *Amino Acids* **2004**, *26*, 139−146.
(36) Girgis, A. S.; Tala, S. R.; Oliferenko, P. V.; Oliferenko, A. A.; Katritzky, A. R. Computer-Assisted Rational Design, Synthesis, and Bioassay of Nonsteroidal Anti-inflammatory Agents. *Eur. J. Med. Chem.* **2012**, *50*, 1−8.
(37) Abou-Seri, S. M.; Abouzid, K.; Abou El Ella, D. A. Molecular Modeling Study and Synthesis of Quinazolinone-arylpiperazine Derivatives as α_1-Adrenoreceptor Antagonists. *Eur. J. Med. Chem.* **2011**, *46*, 647−658.
(38) Ramesh, B.; Rao, B. S. Synthesis, Spectral Studies and Anti-inflammatory Activity of 2-Acetyl Thiophene. *E-J. Chem.* **2010**, *7*, 433−436.
(39) Turan-Zitouni, G.; Özdemir, A.; Güven, K. Synthesis of Some 1-[(*N, N*-Disubstituted thiocar bamoylthio)acetyl]-3-(2-thienyl)-5-aryl-2-pyrazoline Derivatives and Investigation of their Antibacterial and Antifungal Activities. *Arch. Pharm. (Weinheim, Ger.)* **2005**, *338*, 96−104.
(40) Greiner-Bechert, L.; Otto, H. H. 1,4-Pentandien-3-ones, XXXII: Reaction of 2-Acetylthiophene and 2-Acetylfuran with Malononitrile and Aldehydes, and Synthesis and Properties of Phenylene-bis[(thienyl/furyl)nicotinonitrile] Derivative. *Arch. Pharm. (Weinheim, Ger.)* **1991**, *324*, 563−572.